Dynamics Modeling and Real-Time Observation of Galvanotaxis in *Paramecium caudatum* towards Robotic Maneuvering

Naoko Ogawa[a,*], Hiromasa Oku[a], Koichi Hashimoto[b] and Masatoshi Ishikawa[a]
[a]Graduate School of Information Science and Technology, University of Tokyo
[b]Graduate School of Information Sciences, Tohoku University

***Abstract*— Paramecium caudatum, a kind of ciliates, exhibits very strong galvanotaxis; When a DC electric field is applied, cells are forced to swim toward the cathode. In this paper, we propose a novel physical scheme for Paramecium galvanotaxis to provide a quantitative explanation for the Ludloff phenomenon, using a bottom-up approach based on systems theory. Our goal is to utilize microbes as micro-robots, and the proposed model would be effective for maneuvering cells. We analytically derived this torque with respect to the cell angle, and constructed equations of translational and rotational motions. Using the proposed model, we performed numerical simulations. We also performed a preliminary evaluation of the proposed model by using real data. Experimental data were obtained by high-speed measurement of the responses of a single cell to an electric field, using the galvanotaxis continuous measurement system developed originally. It was found that the simulated data was approximately in agreement with the experimental results.**

Keywords: **Paramecium, galvanotaxis, microrobot, dynamics model**

I. Introduction

Today, there is great interest in measurement and control at the micrometer and nanometer scale. Conventional methods, however, have required human operators with high dexterity, expertise, and long experience. Hence, automation technologies to assist operators are needed. Yet, there remain many problems to be solved before its practical application becomes realistic; these problems are mainly due to the still relatively young and undeveloped nature of the field and the limited technology available.

Our approach to overcome these problems is to utilize naturally occurring micromachines, or microorganisms. For all living things, detection of changes in the environment and quick reaction are essential for their survival. Therefore, microorganisms have acquired sophisticated sensors and actuators through the course of their evolution. If we can develop techniques to control them freely, we can realize multi-purpose, programmable microrobotic systems superior to existing micromachine systems. Our goal is to eventually integrate controlled microorganisms and information processing systems [1]. By controlling microorganisms, we aim to achieve various applications, such as cell manipulation, microscopic delivery, smart microsensors, and assembly of micro-electro mechanical systems (MEMS).

To develop microrobotic applications of microorganisms, actuation, navigation and maneuvering of cells are key technologies to be realized first. One effective candidate for actuation would be to utilize galvanotaxis, an intrinsic locomotor response to an electrical stimulus, because of its non-invasive and non-contact nature. Using galvanotaxis, some recent studies have achieved simple motion control of *Paramecium caudatum*, a kind of protozoa with strong galvanotaxis [1–3]. However, these studies were based on simple empirical rules without knowledge about the physical properties of the cells, and thus had limited control performance.

To realize more precise maneuver, it is essential to deal with Paramecium in the framework of standard robotics, that is, to discuss its dynamics, trajectory planning, advanced motion control and so on. The minimal and most basic preparation required for this discussion is a mathematical and quantitative model of the physical dynamics of Paramecium. The purpose of this paper, therefore, is to propose a novel physical scheme for Paramecium galvanotaxis to provide a quantitative explanation for the Ludloff phenomenon and to utilize it for robotic maneuvering, using a bottom-up approach.

Although several properties of Paramecium cells have been modeled, conventional models have mainly been physiological and biochemical ones that have focused on the membrane potential or signal transduction, ignoring the physical properties [4], [5]. Moreover, the few physical models that have been presented have tended to disregard galvanotaxis. One rare physical model of galvanotaxis is that constructed by Roberts [6]; however, its validity is uncertain because his assumptions were rough, and the accuracy of his model was not fully verified by comparing it with experimental data. This paper is the first attempt to construct a physical model of Paramecium galvanotaxis based on mechanics using a bottom-up approach, accompanied with experimental validation.

II. Dynamics Model of Paramecium Galvanotaxis

A. Paramecium and Its Galvanotaxis

In this paper, we consider *Paramecium caudatum* because it has been extensively studied and its behavior is well known. *P. caudatum* is a unicellular protozoan with an ellipsoidal shape,

*Corresponding author: 7–3–1 Hongo, Bunkyo-ku, Tokyo 113–8656, Japan. Tel: +81–3–5841–6937, Fax: +81–3–5841–6952, E-mail: Naoko_Ogawa@ipc.i.u-tokyo.ac.jp

inhabiting freshwater. It swims by waving cilia on its body; thousands of cilia beat the water backward to yield a forward reaction force [7]. The ciliary motion is controlled by shifts in the membrane potential and the accompanying changes in ion concentration in the cell.

When an external electrical stimulus is applied, it modifies the membrane potential and alters the ciliary movements, thus affecting the cell motion. Viewed macroscopically, the cell is made to swim toward the cathode. This phenomenon is called negative galvanotaxis. Note that galvanotaxis is simply a side-effect of the electrophysiological nature of the cell, unlike chemotaxis and phototaxis, which are behaviors conferring a survival advantage.

A Paramecium cell in an electric field shows a characteristic ciliary movement pattern. Assume an imaginary plane that is perpendicular to the electric field and located near the center of the cell, slightly closer to the cathodal end, dividing the cell into two parts, as illustrated in Fig. 1. The electric field causes cilia on the anodal end to beat more frequently (ciliary augmentation) [8], and the cilia on the cathodal end also beat more frequently but in the opposite direction (ciliary reversal) [9]. This is called the Ludloff phenomenon [9], and it provides a simple and qualitative explanation for galvanotaxis: the asymmetry in direction of the ciliary beatings generates a rotational force and orients the cell toward the cathode.

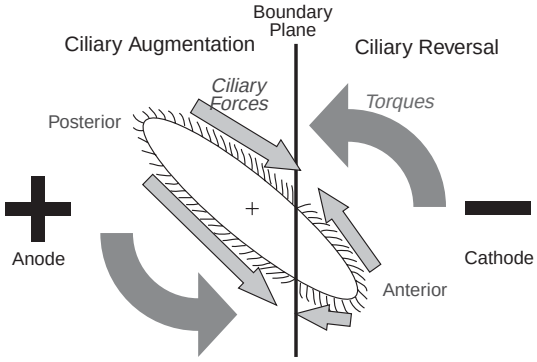

Fig. 1. Qualitative explanation for galvanotaxis.

Based on electrochemical and electrophysiological knowledge [4], [5], the mechanism of the Ludloff phenomenon can be understood to be a combination of electrochemical, physiological and physical factors. Electrochemical and physiological factors have mainly been considered in previous studies. However, much remains unknown, and further theoretical studies cannot proceed without experimental data elucidating the structural and biochemical properties. On the other hand, though physical factors have not been considered sufficiently, they play an essential role in galvanotaxis and may be well described using simple physics. This paper concentrates on physical factors, while regarding electrochemical and physiological factors as "black boxes".

B. Assumptions

By making several assumptions focusing only on those properties that are essential and dominant in galvanotaxis [10], we can describe the cell motion in a two-dimensional plane

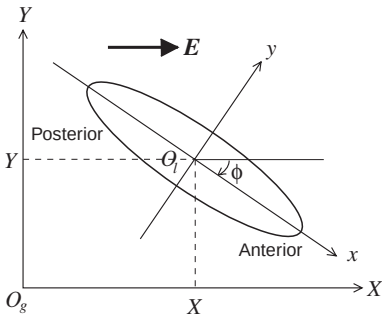

Fig. 2. The global coordinate system (X, Y).

including the cell axis and the electric field vector. Hereafter, we consider cell motion only in this plane. Also, we can consider the cell as a two-dimensional ellipsoid on this plane.

We define a global coordinate system (X, Y) and a local coordinate system (x, y) on the plane, as shown in Figure 2. The global coordinate system is fixed with respect to the external world, with the X-axis parallel to the electric field $\boldsymbol{E}$. Let ϕ be the angle of the cell axis in the global coordinate system ($\phi < 0$ in Figure 2, for the sake of convenience in deriving the model). The local coordinate system is fixed with respect to the cell.

Let the cell shape be an ellipsoid $\mathcal{E}$ with a major axis of length $2L$ and a minor axis of length $2R$ ($L > R$). In the local coordinate system, the cell is represented as an ellipsoid $\mathcal{E}$:

$$\mathcal{E} : \frac{x^2}{L^2} + \frac{y^2}{R^2} = 1. \tag{1}$$

We assume that cilia are distributed uniformly around the edge of the ellipsoid with linear density n. In the presence of an electric field, imagine a plane perpendicular to the field (hereinafter referred to as "a boundary plane"). The shortest distance between the plane and the center of the cell is set to l.

The propulsion force yielded by one cilium is assumed to be f_0 in the absence of an electric field. In the presence of an electric field E, the force increases to $f = (1+\beta E) f_0$, where β is a positive parameter.

C. Model of the Torque

The phenomenon whereby a Paramecium cell swims toward the cathode is due to a torque caused by asymmetry of ciliary motion. In this section, we estimate this torque. First, consider an ellipsoid $\mathcal{E}$ in the local coordinate system, as illustrated in Fig. 3. Note that the following model is defined only if $\boldsymbol{E} \neq \boldsymbol{0}$.

For convenience, let us introduce $\theta = -\phi$ as the angle of the electric field $\boldsymbol{E}$ in the local coordinate system. Then the boundary plane is expressed as a line $\mathcal{L}$:

$$\mathcal{L} : y = -\frac{1}{\tan\theta} x + \frac{l}{\sin\theta}. \tag{2}$$

The asymmetry of ciliary beating exists only at the substantially trapezoidal region formed by the intersection of the boundary plane and the ellipsoid (shown as the hatched region in Fig. 3. Draw two lines parallel to y-axis from the two intersection points of $\mathcal{E}$ and $\mathcal{L}$, and you will get two more

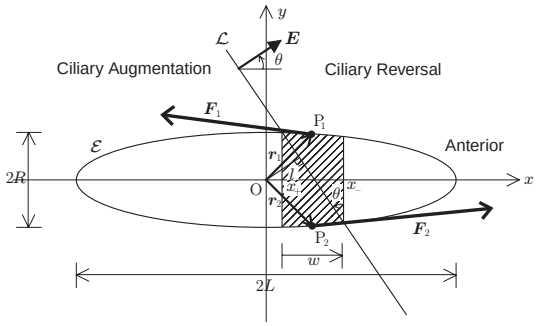

Fig. 3. The local coordinate system. Only the cilia on the hatched trapezoidal region contribute to the rotation.

intersecting points. The resulting four points make up the trapezoid). The forces yielded by cilia outside this region are symmetrical and do not contribute to rotation. Thus, we have only to consider the forces generated at this trapezoidal region.

The x-coordinates of two vertical lines that define the "upper" side and "lower" side of the trapezoid (that is, the sides parallel to the y-axis) are equal to those of two intersecting points of $\mathcal{E}$ and $\mathcal{L}$. These two coordinates, x_- and x_+, are obtained as two roots of the equation derived by eliminating y from Eq. (1) and Eq. (2) (obviously this equation always has two real roots). Let x_+ be the x-coordinate of the point with the larger y-coordinate and x_- be the x-coordinate of the point with the smaller y-coordinate.

Because it would be too complicated to consider the individual minute forces generated by each cilium, here we focus on the resultant forces for simplicity. We set sites of action, $\mathrm{P}_1(x_\mathrm{a}, y_\mathrm{a})$ and $\mathrm{P}_2(x_\mathrm{a}, -y_\mathrm{a})$, at the midpoints of the sides of the trapezoid and assume the directions of the forces to be tangential to the ellipsoid. We then define position vectors, $\boldsymbol{r_1} = \overrightarrow{\mathrm{OP}_1}$ and $\boldsymbol{r_2} = \overrightarrow{\mathrm{OP}_2}$. Next, let us suppose that the magnitude of the resultant force is proportional to the "height" of the trapezoid w, which is a signed value the same sign as θ. Then, the propelling forces $\boldsymbol{F}_1$ and $\boldsymbol{F}_2$ at the points P_1 and P_2, respectively, are represented by $\boldsymbol{F}_{\{1,2\}} = \mp fwn\boldsymbol{m}_{\{1,2\}}$, where $\boldsymbol{m}_1$ and $\boldsymbol{m}_2$ are the unit tangent vectors at P_1 and P_2, and the $\mp$ symbol indicates the two directions of ciliary beating. Thus, we find the torques at the points $\mathrm{P}_{\{1,2\}}$, namely, $\boldsymbol{\tau}_{\{1,2\}} = \boldsymbol{r}_{\{1,2\}} \times \boldsymbol{F}_{\{1,2\}}$. It should be noted that these vectors are treated as three-dimensional in calculating cross products. The total torque rotating the cell body is given by $\boldsymbol{\tau} = \boldsymbol{\tau}_1 + \boldsymbol{\tau}_2$. Since its x and y components are obviously zero, hereafter we call its z component, τ_z, the "torque".

Finally, by substituting $\phi = -\theta$, the torque is described in the global coordinate system as:

$$\tau_z(\phi) = -\frac{4LR^2 fns\sqrt{L^2c^2 + R^2s^2 - l^2}}{\sqrt{L^4c^4 + 2L^2R^2c^2s^2 + R^4s^4 - L^2l^2c^2 + R^2l^2c^2}}, \tag{3}$$

where $s = \sin\phi$ and $c = \cos\phi$. This equation describes the torque generated in the cell oriented at the angle ϕ.

D. Forward Propulsion Force

As mentioned above, only the cilia on the trapezoid contribute to the rotation. Other cilia are responsible for translational propulsion. Considering that the reversed effective strokes on the cathodal side produce a backward force, we can derive the magnitude of the force F as:

$$F = \begin{cases} 2fn|x_a| & (|L\cos\theta| > 1), \\ fn(2L - |w|) & (|L\cos\theta| < 1). \end{cases} \tag{4}$$

E. Equations of Motion of Paramecium Cell

Using the torque estimated in section II-C, we now discuss the equations of motion of the Paramecium cell.

In the micrometer-scale world that paramecia inhabit, the inertial resistance of the fluid is small enough to be negligible, and the viscous resistance becomes dominant. Hence we can apply Stokes' law, derived from the Navier-Stokes equation by ignoring inertial force.

Since a rigorous evaluation of the viscous resistance around an ellipsoid is quite complicated, here we approximate the viscosity by applying the formula for a sphere as a substitute. According to Stokes' law, the force exerted on a sphere with radius a, moving with velocity v in a viscous fluid is given by $F_\mathrm{s} = 6\pi\mu av$, where μ is the viscosity of the fluid. From this equation, the viscous force around the ellipsoidal cell can be obtained by replacing the radius a by the cell radius R. Thus the equation of motion for the translational motion of the cell can be approximated by:

$$M\ddot{\boldsymbol{X}} + D\dot{\boldsymbol{X}} = \boldsymbol{F}, \tag{5}$$

where $\boldsymbol{X} = (X, Y)^\mathrm{T}$ is the cell position (a superscript T means the transposition), $\boldsymbol{F} = F\boldsymbol{e}$ is a forward propulsive force, $\boldsymbol{e} = (\cos\phi, \sin\phi)^\mathrm{T}$ is a unit vector along the body axis, $D = F_\mathrm{s}/|\dot{\boldsymbol{X}}| = 6\pi\mu R$ is the viscous friction coefficient, $M = \rho V$ is the cell mass, ρ is the cell density, and $V = 4\pi LR^2/3$ is the cell volume.

Next, we derive an equation of motion for the rotational motion. As mentioned above, because evaluation of the viscosity around the ellipsoid is too complicated, we again substitute Stokes' law for a sphere. A viscous resistance torque against the rotation can be roughly approximated by assuming two mass points on the longitudinal axis at a quarter of the length $(L/2)$ from the origin, substituting $v = \dot{\phi} \cdot L/2$ and $a = L/2$ into the Stokes' law equation, and multiplying both sides by $L/2$:

$$\tau_\mathrm{s} = 2 \times F_\mathrm{s}\frac{L}{2} = 12\pi\mu\frac{L}{2}\dot{\phi}\frac{L}{2}\frac{L}{2} = \frac{3}{2}\pi\mu L^3\dot{\phi}.$$

This derivation, however, may be too rough and the coefficient $3/2$ might be unreliable, which may cause significant error in the model. Therefore, we introduce coefficient δ instead of the coefficient $3/2$ to compensate for the error. Thus, the equation of motion for the rotational motion is given by

$$I\ddot{\phi} + D'\dot{\phi} = \tau_z(\phi), \tag{6}$$

where $I = \pi M(R^2 + L^2)/5$ is the moment of inertia for an ellipsoid, and $D' = \tau_\mathrm{s}/\dot{\phi} = \delta\pi\mu L^3$ is the viscous friction coefficient.

TABLE I

PARAMETERS OF THE PROPOSED MODEL.

Parameters	Values	Comments
Major cell axis $2L$	100μm	our strain
Minor cell axis $2R$	25μm	our strain
Boundary plane offset l	10μm	[11], [12]
Viscosity of water μ	1.00×10^{-3} kg/(ms)	at 20 ℃
Cell density ρ	$1,000$ kg/m^3	same as water
Increase in beating freq. β	2.00×10^{-3} V^{-1}	

Finally, integration of the equations of motion for the translational motion and the rotational motion leads to the following equations with a notation common in systems theory:

$$\dot{\boldsymbol{q}} = A\boldsymbol{q} + \boldsymbol{B}(\boldsymbol{q}), \tag{7}$$

$$A = \begin{pmatrix} 0 & 0 & 1 & 0 & 0 & 0 \\ 0 & 0 & 0 & 1 & 0 & 0 \\ 0 & 0 & -D/M & 0 & 0 & 0 \\ 0 & 0 & 0 & -D/M & 0 & 0 \\ 0 & 0 & 0 & 0 & 0 & 1 \\ 0 & 0 & 0 & 0 & 0 & -D'/I \end{pmatrix},$$

$$\boldsymbol{B}(\boldsymbol{q}) = \left(0, 0, \frac{F}{M}\cos\phi, \frac{F}{M}\sin\phi, 0, \frac{\tau_z(\phi)}{I}\right)^{\mathrm{T}},$$

where $\boldsymbol{q} = (X, Y, \dot{X}, \dot{Y}, \phi, \dot{\phi})^{\mathrm{T}}$.

III. NUMERICAL EXPERIMENTS

We performed some numerical experiments to verify the equations of motion using numerical analysis software (MATLAB, MathWorks Inc.).

A. Physical Parameters

Table I shows several physical parameters used in the numerical experiments. We obtained the cell size by observing cells incubated in our laboratory; the size we observed was smaller than the average reported by Jennings [11]. The boundary plane offset l was estimated from several illustrations shown in previous studies [11], [12]. The value of β, the increase in beating frequency with electric field, was estimated from the fact that the frequency increased to around 50 Hz under a stimulation of a few volts per centimeter from the frequency in the regular state of around 15-20 Hz [7].

The force yielded by cilia on the unit length, $f_0 n$, is still an unknown parameter. For rigorous evaluation, we might have to consider the physical model of a cilium [13] and its interaction with the surrounding fluid. However, our model itself is based on approximation, and a strict evaluation of $f_0 n$ is not so critical. Hence we estimated the order of $f_0 n$ by using the swimming velocity measured in past experiments.

The terminal velocity of a cell was obtained by substituting $\ddot{\boldsymbol{X}} = \boldsymbol{0}$ into eq. (5) under conditions of $\phi = 0$:

$$\dot{\boldsymbol{X}} = \boldsymbol{F}/D = \frac{|x_a|_{\phi=0}\boldsymbol{e}}{3\pi\mu R} f_0 n. \tag{8}$$

Since x_a equals l at $\phi = 0$, we can estimate $f_0 n$ from:

$$f_0 n = \frac{3\pi\mu R}{l}|\dot{\boldsymbol{X}}|. \tag{9}$$

Measurement of the cell velocity by using a high-speed tracking system [14] described later in section *IV-C*, gave a velocity of around 400μm/s. Using this value, we estimated $f_0 n$ to be 4.71×10^{-6} N/m. In addition, we adjusted the parameter δ to be 7.5 based on experimental data of the cell trajectories obtained by our system [15].

B. Torque Profile

Fig. 4 shows the torque $\tau_z(\phi)$ as a function of ϕ. Note that the torque affects the cell so as to decrease ϕ, that is, to make the cell turn toward the cathode.

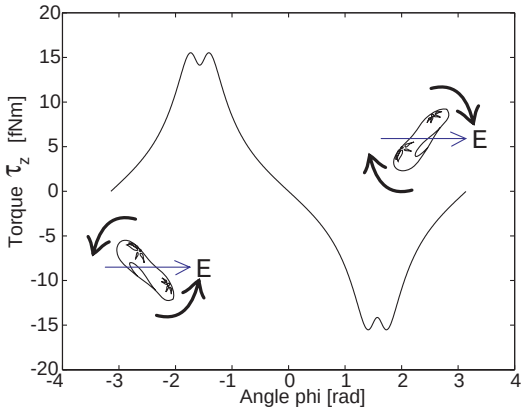

Fig. 4. Torque $\tau_z(\phi)$ generated by ciliary force. When $\phi > 0$, a negative torque is generated to rotate the cell clockwise. When $\phi < 0$, a positive torque is generated to rotate the cell counterclockwise. In both cases, the cell is eventually oriented toward the cathode.

These results indicate that the orientations $\phi = \pm\pi$ are kind of "singular point" where no torque is produced, even though the cell is oriented toward the anode. This means that such a cell will move towards the anode, which seems inconsistent with the observed behavior of negative galvanotaxis. In practice, however, swimming paramecia always sway slightly. The slight swaying of the cell generates a torque, causing the cell to incline further. This positive feedback rotates the cell and eventually directs it toward the cathode.

Also, the global stability of the cell angle was verified qualitatively by calculating a potential energy U for rotation. We defined U as

$$\tau_z = -\frac{\partial U}{\partial \phi}$$

and computed it by numerical integration of Eq. (3) with respect to ϕ. Fig. 5 shows the profile of U, indicating that the cell is stable and tends to approach $\phi = 0$ for all ϕ.

C. Simplification of Equations

In the micrometer-scale world that the Paramecia inhabit, the inertia terms ($M\ddot{X}$, $M\ddot{Y}$ and $I\ddot{\phi}$) are much smaller than the viscosity terms ($D\dot{X}$, $D\dot{Y}$ and $D'\dot{\phi}$) because of the small Reynolds number. In fact, M is 2.62×10^{-10}, which is much

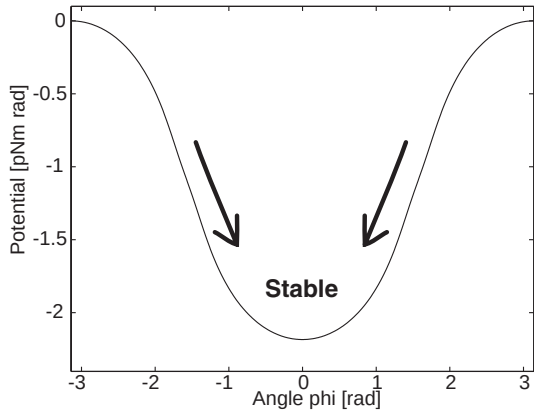

Fig. 5. Potential energy versus torque, obtained by numerical integration of $\tau_z(\phi)$. The potential is minimized only at $\phi = 0$, indicating that the cell tends to approach $\phi = 0$ for all ϕ.

smaller than $D = 4.71 \times 10^{-7}$, and I is 1.74×10^{-18}, which is much smaller than $D' = 2.35 \times 10^{-14}$. We performed simulation without the inertial terms and found that the results were almost the same as those obtained with the inertial terms. Thus, the equations of motion can be approximately simplified by ignoring the inertial terms as follows:

$$D\dot{X} = F\cos\phi,\ D\dot{Y} = F\sin\phi,\ D'\dot{\phi} = \tau_z(\phi).$$

The following simulations were performed without inertia terms.

D. Emergence of U-Turn Motion

When an electric field is applied in the direction opposite to the swimming direction of a cell, the cell makes a U-turn motion. We tested whether our proposed model can exhibit this phenomenon like real cells.

Swimming trajectories for cells with eleven different initial orientations were calculated. Fig. 6 demonstrates all trajectories simultaneously. All cells were configured to have the same initial position, namely, on the origin $(0, 0)$, but their initial angles ϕ differed by intervals of 30°($-150°, -120°, \ldots, 150°$). An electric field of 5.0 V/cm was applied along the X-axis. The trajectory of each cell was calculated by solving ordinary differential equations. As shown in Fig. 6, all cells starting from the origin turned toward the cathode, like real cells. It is interesting that realistic macroscopic behavior emerged from a microscopic description of the ciliary motion.

E. U-turn Motion with Spiral Term and Noise Term

When the cell inclination ϕ is close to $\pm\pi$, Fig. 4 indicates that the torque is so small that the cell might fail to make an U-turn, or might need an extremely long time to turn. Actually, however, cells are certain to make an U-turn within short time. We think that it is due to the spiral path, as well as the perturbation of the cell angle caused by a noise. In this section, we consider incorporating a spiral motion, along with a noise term, into the simulation.

As mentioned above, the actual cell swims spinning along a spiral. The spiral path can be expressed as a sine curve [7].

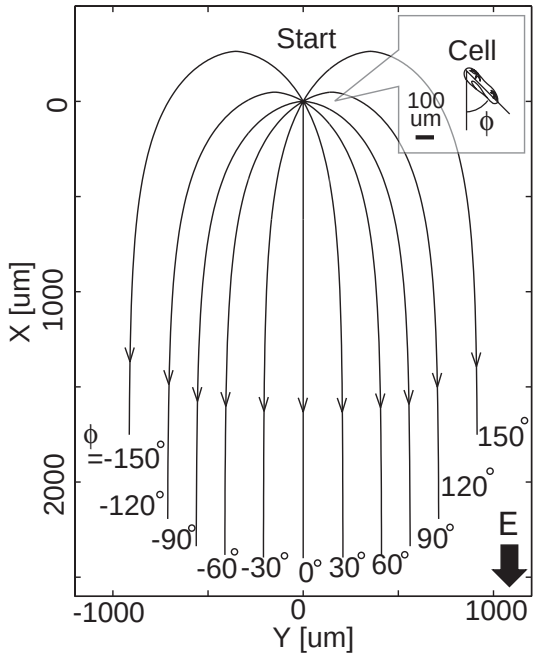

Fig. 6. Simulation of U-turn motions of cells.

To put it simply, it is written as:

$$\bar{X} = V_{\bar{X}}t,\ \bar{Y} = V_{\bar{Y}}\cos\omega t,$$

where $\bar{X}$ correspond to the spiral axis whose direction is always oriented to the cell inclination ϕ, $\bar{Y}$ is an axis perpendicular to $\bar{Y}$, $V_{\bar{X}}$ and $V_{\bar{Y}}$ are amplitude coefficients, ω is the angular velocity, and t is time. Let $\bar{\phi}$ the cell inclination with respect to the $\bar{X}$ axis. Then,

$$\tan\bar{\phi} = \frac{\mathrm{d}\bar{Y}}{\mathrm{d}\bar{X}} = -\omega\frac{V_{\bar{Y}}}{V_{\bar{X}}}\sin\frac{\omega}{V_{\bar{X}}}t,$$
$$\bar{\phi} = \arctan(-\omega\frac{V_{\bar{Y}}}{V_{\bar{X}}}\sin\frac{\omega}{V_{\bar{X}}}t).$$

Because the spiral axis, or $\bar{X}$ axis, is always oriented to the swimming direction ϕ, the resulting cell angle is expressed as the sum of the path term ϕ and the spiral term $\bar{\phi}$: $\phi \leftarrow \phi + \bar{\phi}$. Finally, by considering a noise term N, the cell angle ϕ can be roughly enhanced as $\phi \leftarrow \phi(1 + N)$.

We performed a numerical experiment. ω was set to be 2 according to the measurement [15]. We also set N as a brown noise with the magnitude of 8.0×10^{-9}, and $V_{\bar{X}} = V_{\bar{Y}} = 1$. Other parameters were same as the U-turn experiment in Sec. III-D. The initial angle was set to be $180°$, which means that the cell was oriented to the anode.

Fig. 7 shows simulated trajectories for 10 trials. All cells made a full 180-degree U-turn motions and swam toward the cathode along the spiral path, although the torque was zero at the initial point.

F. Shape-Dependent Behavior Dynamics

In the numerical experiments described above, the parameter values were average values of multiple observed cells. However, there is significant intercellular variation, which may

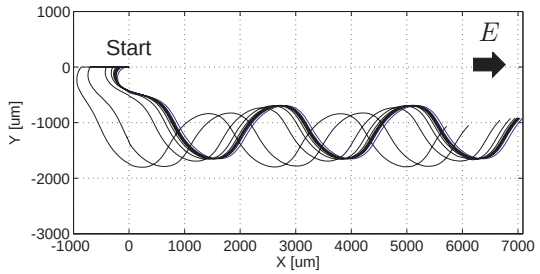

Fig. 7. Simulation of U-turn motions with a noise term and a spiral term for 10 different trials. All cells made a full 180-degree U-turn motions and swam toward the cathode along the spiral path, although the torque was zero at the initial point.

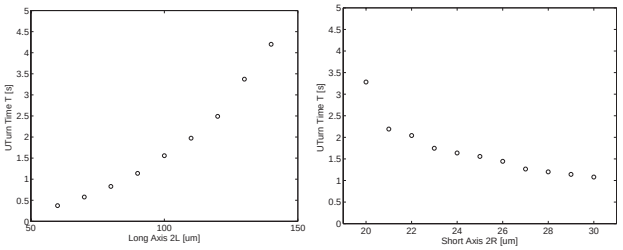

Fig. 8. Relationship between U-turn time and (a) L and (b) R. These graphs indicate that it takes more time for elongated cells to make a U-turn.

affect the macroscopic behavior. As an example, we varied the size parameters R and L to examine the effect on the behavior dynamics.

Fig. 8 shows the relationship between U-turn time and (a) L and (b) R. R was fixed to be 12.5μm in (a) and L was fixed to be 50μm in (b). It takes more time for more elongated cells to make a U-turn; this is thought to be because elongated shapes experience more resistance in rotation than spherical ones do.

Rotation and translation are quite common motions for paramecia, though their origin is not galvanotactic. The ellipsoidal shape of cells might be the result of evolution, with the trade-off that elongated bodies are favorable for translation but adverse for rotation.

It is implied that the shape deviation cannot be neglected for rigorous evaluation, though it gives almost no fundamental difference in the structure of the model and emerging behaviors. Note that our Stokes-like assumption in motion of equations has to be reconsidered from the hydrodynamic viewpoint if more rigorous discussion is needed, which is not dealt with in this paper.

IV. Real-Time Observation System and Wet Experiments

We have developed a novel system for real-time continuous observation of the microbe galvanotaxis using visual tracking method. In this section, we describe the system. Using this system, we verified the validity of the model using these data.

A. Why Tracking?

To realize free and precise control of cells, some requirements for the observation are: (1) continuous observation of quickly swimming cells with no fixation, (2) a sufficiently large working area for free control, and (3) detailed observation of a specific cell with high magnification for precise actuation.

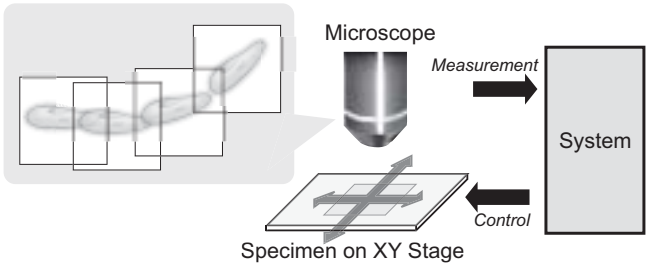

Fig. 9. Lock-on tracking scheme. The camera pursues a target so as to keep it always in the center of the visual field.

We found, however, that most conventional microscope systems, could not satisfy these demands: (1) Continuous observation was quite difficult, because cells swim very quickly. Instead, physical or physiological fixation had to be performed on the cells. (2) The working area was limited to inside of the visual field. (3) So as not to lose cells, we were compelled to observe them with low magnification, thus preventing detailed observation of the cell properties.

To overcome these obstacles, we adopted a tracking method. In this paper, we mainly use the term "tracking" in the sense that the camera pursues a target so as to keep it always in the center of the visual field (sometimes we also call it "lock-on tracking"), while in general, the term "tracking" has a wider meaning, such as just locating the position of moving targets, or extracting targets from a background. As shown in Fig. 9, a lock-on mechanism can be realized by moving the position of the specimen on a stage so that the camera always keeps the target at the center. Although this can also be achieved by moving the camera and the microscope, we did not adopt this technique because it was much easier to move the stage.

Our system measures the cell position and angle continuously at a 1-kHz frame rate, using a high-speed lock-on tracking method.

B. System Configuration

The configuration of the overall system and its block diagram are illustrated in Fig. 10. An electrical stimulus is applied to cells swimming in a chamber on an electrical stimulus input device mounted on an XY stage. The stage is controlled by a high-speed vision system so as to keep a cell in the center of the field of view. By reading encoders on the stage and performing coordinate transformation, we can obtain the global position of the cell. The orientation of the cell is also calculated from image features.

1) Vision System: For the vision system, a high frame rate is required in order not to lose the target at high magnification. Moreover, an observing method with weak light, such as dark field microscopy, is needed so as to prevent heat and light influence on the cells.

To obtain dark images very quickly, we adopted a so-called I-CPV system jointly developed by Hamamatsu Pho-

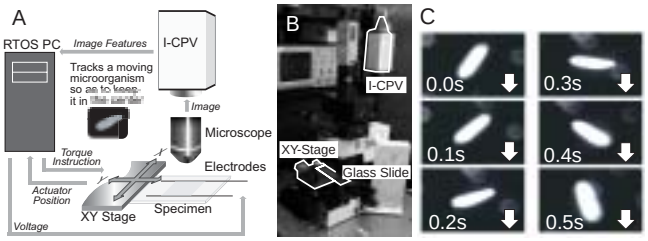

Fig. 10. Experimental setup of our tracking system. A: Schematic overview of the galvanotaxis continuous observation system [16]. B: Photograph of the system. C: An example of U-turn motion monitored by our system.

tonics K.K. and one of the authors of the present paper (Ishikawa) [17]; this is a Column Parallel Vision (CPV) system with an image intensifier. CPV is a high-speed vision system developed for robotic applications [18].

I-CPV captures and processes an 8-bit gray-scale image with 128×128 pixels and 1-kHz frame rate. I-CPV has a 128×128 photo-detector (PD) array and the same number of programmable general-purpose processing elements (PEs). The captured image is amplified several thousand times by the image intensifier and transmitted by a CMOS sensor module (consisting of the PDs and A-D converters) to the PEs in a column-parallel manner. Each PE is based on the S^3PE architecture [19], which adopts a SIMD-type program control, and can process image data completely in parallel. Each PE is connected with a summation circuit, so that it can execute various processes, such as global image feature extraction, edge extraction, embossing and blurring, within 1 ms.

In the system proposed here, the I-CPV system is mounted on an upright optical microscope (Olympus, BX50WI) and captures dark-field images. The images are also captured by a CCD camera for convenience of monitoring. From the captured images, the I-CPV calculates image moments and sends them to the PC. These features are used for calculating the attitude and the position of the target for the visual feedback control of the XY stage and microorganisms. Fig. 10 C shows an example of the tracked image of a Paramecium cell making a U-turn.

The error values in displacement of the target are used to obtain the desired position of the XY stage.

The tracking method introduced above does not work appropriately when there are two or more cells in the field of view. To solve this problem, segmentation of multiple cells and matching of the target between frames are realized by an algorithm called self-windowing [20], using some of the intrinsic characteristics of high-speed imaging.

2) XY Stage: The PC controls the position of a chamber fixed on the XY stage by sending instructions to the stage. The XY stage (SMC, LAL00-X070) has two orthogonal axes, X and Y, whose stroke is 25 mm. Each axis has a linear coil actuator to control the stage position. It also has encoders with 1 μm precision on each axis. By controlling the stage according to the extracted target position, as described later, lock-on tracking of the target is achieved.

3) Electrical Stimulus Input Device: In the electrical stimulus input device, two carbon electrodes of 0.5-mm diameter are placed in parallel on a glass slide, so that we can control

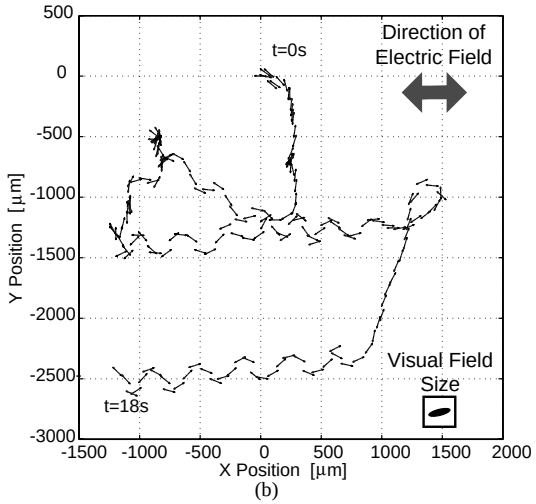

Fig. 11. An example of trajectory and orientation of a cell reconstructed by the real-time galvanotaxis observation system [15].

the electrical stimulus in one direction perpendicular to the electrodes. The distance between them is 22 mm. Between the electrodes, there is a chamber 0.17 mm in depth to contain the specimen, The chamber constrains the motion of the cells within a two-dimensional plane. In order to maintain the chamber depth and to suppress evaporation of the medium, a cover glass is placed on the chamber.

4) Control System: The PC provides a voltage in the range ±10 V to the electrodes via a D/A converter board (Interface, PCI-3310). By feedback of the image feature values acquired by the I-CPV, it is possible to control the voltage in real-time according to the target status.

The whole system is controlled with a frequency of 1 kHz by the PC running a real-time OS (800 MHz, ART-Linux). During each cycle, the PC sets the electrical stimulus applied to the microorganisms in the chamber, the I-CPV then captures the image of the target and calculates its feature values, and the PC sends instructions to the XY stage so as to track the target. Fig. 11 shows an example of the trajectory and orientation of a swimming Paramecium cell reconstructed by the real-time galvanotaxis observation system.

C. Experimental Setup

Experimental data were obtained by high-speed measurement of the responses of a single cell to an electric field, using the galvanotaxis continuous measurement system [16]. The setup of the system is illustrated in Fig. 10.

Wild-type *P. caudatum* cells were cultured at 20-25°C in a soy flour solution. Cells grown to the logarithmic or stationary phase (4-10 days after incubation) were collected together with the solution, filtered through a nylon mesh to remove debris, and infused into a chamber. A DC electric field with a step-like temporal profile rising to 4.1 V/cm was applied to the cells. Cell position and angle were continuously measured at a 1-kHz frame rate.

D. Comparison of Data

We compared simulated and experimental positions in the U-turn motion. We extracted positions along the electric field (X direction), because X-disposition is almost independent of fluctuations caused by spiral motions, which we disregarded.

Fig. 12 shows experimental data (thin lines) for three seconds from application of a stimulus (reversal of the electric field) in six trials. In the simulation (thick line), the initial angle was set to 33.6457 degrees, which is the average of angles obtained from previously measured data. The field strength was set to 4.1 V/cm same as the wet experiment. The figure indicates that the simulated data was approximately in agreement with the experimental results.

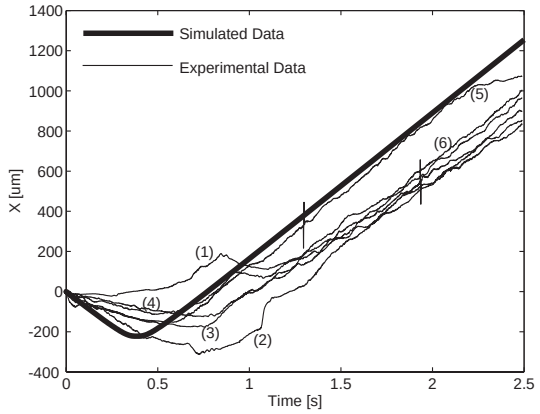

Fig. 12. Comparison between simulated data (thick line) and experimental data (thin lines) in the U-turn motion. Only the X-coordinates (positions along the electric field) are extracted. Experimental data for three seconds from the application of a stimulus in six trials are overlaid. In the experimental results, the initial angles were (1) 58.9055 deg, (2) 20.8729 deg, (3) 22.6034 deg, (4) 36.1584 deg, (5) 29.3349 deg, and (6) 33.9990 deg, respectively. In the simulation, the initial angle was 33.6457, which is the average of six angles obtained from previously measured data. The figure indicates that the simulated data was approximately in agreement with the experimental results.

This comparison is not a strict one because the experimental data represents the projection of real 3-D trajectories onto a 2-D plane. Although the planar structure of the chamber helps to restrict the vertical motion, the cell can still move slightly in this direction. A more rigorous comparison will require three-dimensional tracking. We are developing 3-D tracking methods for our work [21], [22], and experiments are currently underway in our laboratory. Or the disparities might be due to stabilization time for the electrochemical phenomenon, which is supposed to be several hundred milliseconds, or the asymmetrical deviation of the cell shape [23], though they are just a matter for speculation. We are planning to investigate it more precisely by wet experiments.

V. Conclusion

In this paper, we proposed a physical model of Paramecium galvanotaxis using a bottom-up approach to link the microscopic ciliary motion and the macroscopic behavior of a cell, and we investigated the validity of the model by numerical experiments using a novel observation system.

References

[1] N. Ogawa, H. Oku, K. Hashimoto, and M. Ishikawa, "Motile cell galvanotaxis control using high-speed tracking system," in *Proc. 2004 IEEE Int. Conf. Robotics & Automation (ICRA 2004)*, Apr. 2004, pp. 1646–1651.

[2] R. S. Fearing, "Control of a micro-organism as a prototype micro-robot," in *Proc. 2nd Int. Symp. Micromachines and Human Sciences*, Oct. 1991.

[3] A. Itoh, "Motion control of protozoa for bio MEMS," *IEEE/ASME Trans. Mechatronics*, vol. 5, no. 2, pp. 181–188, June 2000.

[4] T. L. Jahn, "The mechanism of ciliary movement. I. Ciliary reversal and activation by electric current; the Ludloff phenomenon in terms of core and volume conductors," *J. Protozoology*, vol. 8, no. 4, pp. 369–380, 1961.

[5] M. S. Cooper and M. Schliwa, "Electric and ionic controls of tissue cell locomotion in DC electric fields," *J. Neuroscience Research*, vol. 13, pp. 223–244, 1985.

[6] A. M. Roberts, "Motion of *Paramecium* in static electric and magnetic fields," *J. Theoretical Biology*, vol. 27, pp. 97–106, 1970.

[7] Y. Naitoh and K. Sugino, "Ciliary movement and its control in *Paramecium*," *J. Protozool.*, vol. 31, no. 1, pp. 31–40, 1984.

[8] T. Kamada, "Control of galvanotropism in Paramecium," *J. the Faculty of Science, Imperial University of Tokyo, Sect. IV, Zoology*, vol. 2, pp. 123–139, 1929.

[9] K. Ludloff, "Untersuchungen über den Galvanotropismus," *Archiv fur die Gesamte Physiologie*, vol. 59, pp. 525–554, 1895.

[10] N. Ogawa, H. Oku, K. Hashimoto, and M. Ishikawa, "Dynamics model of Paramecium galvanotaxis for microrobotic application," in *Proc. 2005 IEEE Int. Conf. Robotics & Automation (ICRA 2005)*, Apr. 2005, pp. 1258–1263.

[11] H. S. Jennings, *Behavior of the Lower Organisms*. Columbia University Press, 1923.

[12] T. Kamada, "Polar effect of electric current on the ciliary movements of Paramecium," *J. the Faculty of Science, Imperial University of Tokyo, Sect. IV, Zoology*, vol. 2, pp. 285–298, 1931.

[13] K. Sugino and Y. Naitoh, "Simulated cross-bridge patterns corresponding to ciliary beating in *Paramecium*," *Nature*, vol. 295, pp. 609–611, 1982.

[14] H. Oku, N. Ogawa, K. Hashimoto, and M. Ishikawa, "Two-dimensional tracking of a motile micro-organism allowing high-resolution observation with various imaging techniques," *Rev. Scientific Instruments*, vol. 76, no. 3, Mar. 2005.

[15] N. Ogawa, H. Oku, K. Hashimoto, and M. Ishikawa, "Microrobotic visual control of motile cells using high-speed tracking system," *IEEE Trans. Robotics*, vol. 21, no. 4, pp. 704–712, Aug. 2005.

[16] ——, "Single-cell level continuous observation of microorganism galvanotaxis using high-speed vision," in *Proc. 2004 IEEE Int. Symp. Biomedical Imaging (ISBI 2004)*, Apr. 2004, pp. 1331–1334.

[17] H. Toyoda, N. Mukohzaka, K. Nakamura, M. Takumi, S. Mizuno, and M. Ishikawa, "1ms column-parallel vision system coupled with an image intensifier; I-CPV," in *Proc. Symp. High Speed Photography and Photonics 2001*, vol. 5-1, 2001, pp. 89–92, in Japanese.

[18] Y. Nakabo, M. Ishikawa, H. Toyoda, and S. Mizuno, "1ms column parallel vision system and it's application of high speed target tracking," in *Proc. 2000 IEEE Int. Conf. Robotics & Automation (ICRA2000)*, Apr. 2000, pp. 650–655.

[19] M. Ishikawa, K. Ogawa, T. Komuro, and I. Ishii, "A CMOS vision chip with SIMD processing element array for 1 ms image processing," in *Dig. Tech. Papers of 1999 IEEE Int. Solid-State Circuit Conf. (ISSCC'99)*, 1999, pp. 206–207.

[20] I. Ishii, Y. Nakabo, and M. Ishikawa, "Target tracking algorithm for 1ms visual feedback system using massively parallel processing," in *Proc. 1996 IEEE Int. Conf. Robotics & Automation (ICRA'96)*, vol. 3, Apr. 1996, pp. 2309–2314.

[21] H. Oku, K. Hashimoto, and M. Ishikawa, "Variable-focus lens with 1-kHz bandwidth," *Optics Express*, vol. 12, no. 10, pp. 2138–2149, 2004.

[22] H. Oku, Theodorus, K. Hashimoto, and M. Ishikawa, "High-speed autofocusing of a cell using diffraction pattern," *Optics Express*, (in press).

[23] Y. Mogami, J. Ishii, and S. A. Baba, "Theoretical and experimental dissection of gravity-dependent mechanical orientation in gravitactic microorganisms," *Biological Bulletin*, vol. 201, pp. 26–33, Aug. 2001.